PROCEEDINGS OF SPIE

SPIEDigitalLibrary.org/conference-proceedings-of-spie

Low-capacitance InGaAs detectors for high-speed, wide field-of-view sensing applications

Jon Geske, Andrew Hood, Jeremy Thomas, Michael MacDougal

Jon Geske, Andrew Hood, Jeremy Thomas, Michael MacDougal, "Low-capacitance InGaAs detectors for high-speed, wide field-of-view sensing applications," Proc. SPIE 11002, Infrared Technology and Applications XLV, 1100214 (7 May 2019); doi: 10.1117/12.2521090

SPIE.

Event: SPIE Defense + Commercial Sensing, 2019, Baltimore, MD, United States

Low Capacitance InGaAs Detectors for High-Speed, Wide Field of View Sensing Applications

Jon Geske, Andrew Hood, Jeremy Thomas, Michael MacDougal

Attollo Engineering, LLC, 1260 Avenida Acaso, Suite B, Camarillo, CA 93003

jon.geske@attolloengineering.com

ABSTRACT

Attollo has developed large area low capacitance InGaAs detectors to meet the needs of LiDAR systems following the roadmap of technology development at the near Infrared (NIR) wavelengths of 850/905/940 nm with the eventual transition to eye-safe wavelengths near 1550 nm. Attollo InGaAs offers large photodetector areas while still meeting the bandwidth limitations of the amplified detection system. Large area photodetectors enable a large system Field of View (FOV) with a simpler and larger diameter lens and also provide lower input-referred noise from optimized transimpedance amplifier systems. Attollo will present results on InGaAs detectors achieving capacitance densities 3x lower than state-of-the-art with 16 pF/mm^2. Attollo will present LiDAR receiver modeling data utilizing these detectors and will quantify the advantages of low capacitance in LIDAR applications as it relates to system bandwidth and amplifier input referred noise performance of the system.

BACKGROUND

In the design of optical detection systems such as cameras, free-space optical interconnects, laser warning receivers, laser spot trackers, semi-active laser seekers, rangefinders, and LADAR and LiDAR, large area detectors and detector arrays are of significant value to achieve large fields of view for the optical system. InGaAs is an excellent choice for such detectors when the LiDAR system needs to operate at wavelengths longer than the silicon response cut-off which occurs near 1 um. The wavelength band covered by InGaAs is part of the shortwave infrared band and InGaAs offers high quantum efficiencies to the common eye-safe laser wavelengths from 1.4 um to 1.7 um. Figure 1, taken from Reference [i] shows the relative spectral quantum efficiency of InGaAs detectors. The reference uses the term “VisGaAs” to refers to optical detection without the signal passing through a thick InP substrate or layer. This can be accomplished via substrate removal as discussed in the reference or via front-side illuminated detection as will be discussed in the detectors reviewed in this paper. From Figure 1 we see that the InGaAs quantum efficiency can be above 80% at all the commonly used LiDAR wavelengths near 900 nm and 1500 nm.

Infrared Technology and Applications XLV, edited by Bjørn F. Andresen, Gabor F. Fulop, Charles M. Hanson, Proc. of SPIE Vol. 11002, 1100214

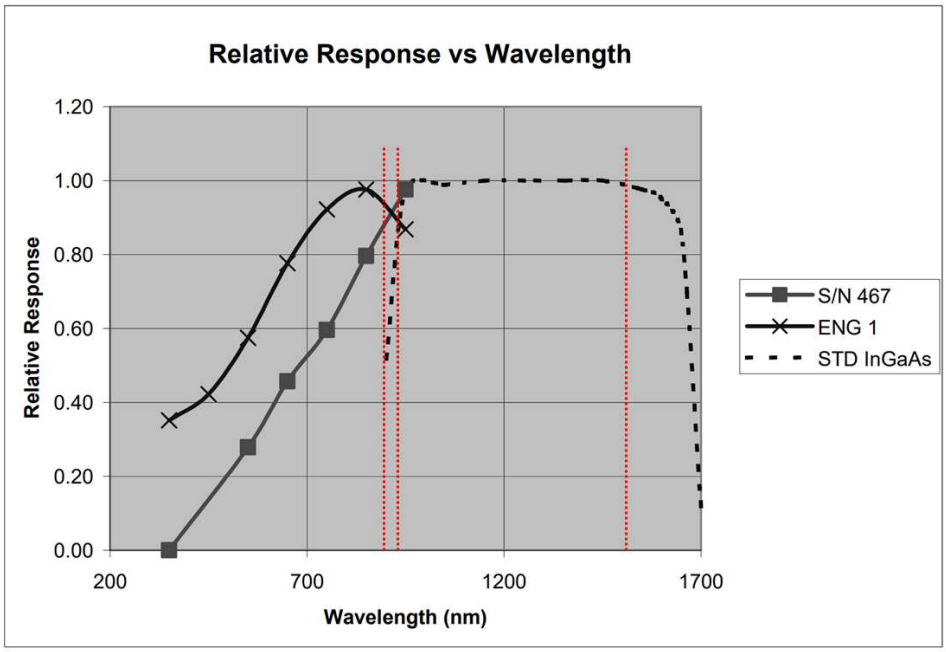

Figure 1. Plot of InGaAs Quantum Efficiency (Reference [i]). Red lines at 905, 940, and 1550 nm added for reference. S/N 467 trace is substrate removed/front-side illuminated InGaAs as used in this paper.

LiDAR systems are a complex collection of optical and electrical components. An example pixel in such a system is shown in Figure 2. Systems include components such as an optical collection element that may focus light onto the photodetector, light blocking filters that limit the wavelengths of light that can reach the photodetector, signal conditioning circuits that prepare the signals produced by the photodetector for subsequent interpretation and manipulation, and decision making circuits that interpret the significance of the signals. In such systems, the application-optimized lens may have a given effective focal length, and the dimensions of the photodetector element or array coupled with the lens determines the angular field of view of the optical detection system.

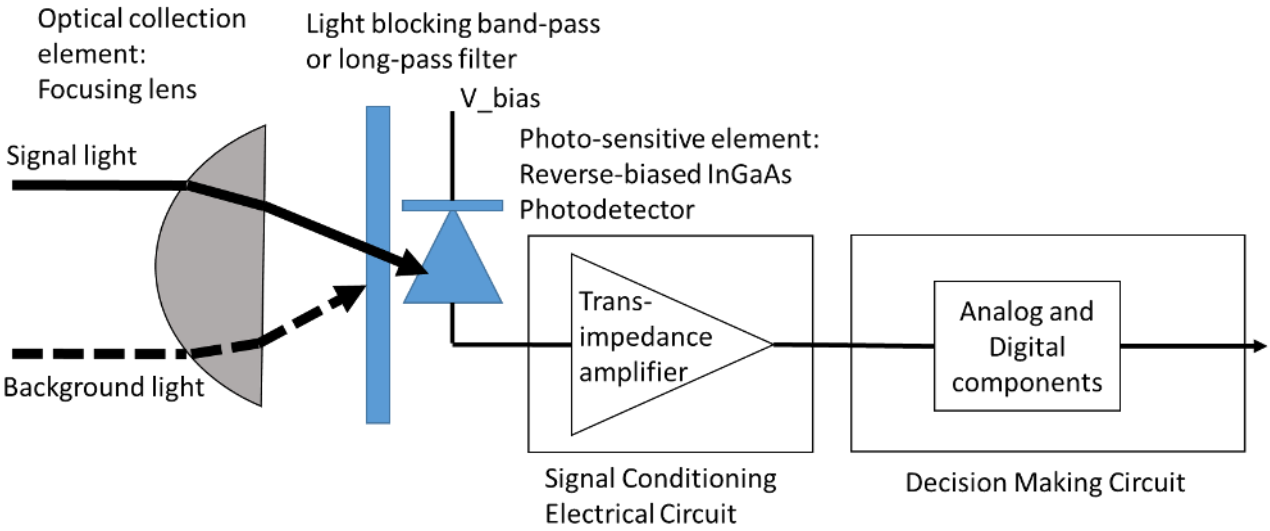

Figure 2. Example topology for an optical detection system

The optical detection system often includes coupling of the signals from the photodetector to a signal conditioning circuit that often includes an electrical amplifier. The amplifier can be configured as a trans-impedance amplifier, taking the photo-generated current from the photo-detector and converting it into a voltage usually with large amounts of gain.

Photodetectors absorb photons and convert them to current that is then delivered to an amplifier circuit. The detector can sometimes be connected directly to the amplifier (Figure 2), and other times it is connected to a Direct Current (DC) blocking capacitor. This is also sometimes called Alternating Current (AC) coupling. The DC-blocking, or AC-coupling capacitor allows only pulsed currents from the detector to enter the amplifier, in accordance with the bandwidth of the AC-coupling circuit parameters. Regardless of the configuration, the amplifier receives a signal from the photodetector that is the result of the absorption of photons. The signal conditioning circuit rarely consists of only a single transimpedance amplifier. Typical passive filters, second and third stage amplification and active filters, level shifting, and many other types of conditioning tasks are performed on the signal.

In such optical detection systems, electrical amplifiers operating with low noise are essential. The noise of the amplifier is an important determining factor in the system sensitivity and hence the ability to detect emitted and reflected light from long distances. The lower the noise of the amplifier, the lower the overall system noise and hence the lower level of light can be detected. In the design of amplifiers, the electrical noise of the amplifier is determined partially by the capacitance of the detector connected to the input of the amplifier. The larger the detector capacitance, the larger the noise at the output of the amplifier.

Many light detection systems are designed to be able to detect fast optical pulses such as from a modulated laser, LED, or other light sources. These systems have electrical amplifiers that have an electrical bandwidth in which they amplify signals. The photodetector converts the optical signals into electrical signals that are then amplified by the electrical amplifier. Signals and noise that have frequency content within the electrical bandwidth of the electrical amplifier are amplified as well. The bandwidth of the electrical amplifier is one of the factors that contributes to the amplifier's output rise time. Signals entering the amplifier that are considerably faster rising than the amplifier's rise time do not significantly increase the rise time of the output. Also signals that are significantly slower than the rise time do not contribute as much to the peak intensity of the output voltage pulse from the amplifier. Maintaining the highest peak intensity of the voltage signal out of the amplifier for a given intensity optical pulse, is one of the primary system level design goals for an optical detection system.

Table 1. Input parameter definitions for TIA bandwidth and nosie governing equations.

C_{IN}	The total input capacitance presented to the TIA
C_D	Photodiode capacitance
C_{CM}	Amplifier common mode capacitance (each input to ground)
C_{DIFF}	Amplifier differential mode capacitance (across the inputs)
C_F	The optimal capacitance to place in the TIA feedback loop
R_F	TIA feedback resistance (sets the gain)
GBWP	The specified gain-bandwidth product of the amplifier used for the TIA
i_n	Amplifier Current Noise Density (A/√(Hz))
e_n	Amplifier Voltage Noise Density (A/√(Hz))
i_{ni}	TIA input referred Noise Density (A/√(Hz))

Equations 1, 2, 3, and 4 from reference [ii] can be used to determine the dependence of the light detection system's noise and bandwidth on the capacitance of the photodetector when operated with a transimpedance amplifier (TIA). Terms for these equations are defined in the Table *1*. This dependence is not entirely obvious to the detector designer and it is instructive to briefly review the impact of the equations.

$$C_{IN} = C_D + C_{CM} + C_{DIFF} \qquad \text{Equation 1}$$

For larger area InGaAs detectors, the photodiode capacitance term will typically dominate in the computation of C_{IN}. Equation 2 and Equation 3 show the buildup of the TIA frequency response performance under the assumption that the TIA feedback resistance is set to the value computed for C_F. This frequency response is strongly dependent on the detector capacitance and this is the attribute most commonly considered by the detector designer.

$$C_F = \sqrt{\frac{C_{IN}}{2\pi(GBWP)R_F}} \qquad \text{Equation 2}$$

$$f_{-3\,dB} \cong \sqrt{\frac{GBWP}{2\pi R_F C_{IN}}} \qquad \text{Equation 3}$$

The LiDAR system designer must concern themselves with the input referred noise of the receiver. This system level noise is determined largely by the TIA noise and Equation 4 instructs the reader that the TIA noise, in units of Amps per root Hz, is dependent on the detector capacitance based on the 4th term of the input referred noise density equation for the TIA. It will be shown later in the DETECTOR PERFORMANCE section of this paper that this term dominates for large area detectors and hence managing the capacitance of the system is important.

$$i_{ni} = \sqrt{i_n^2 + \left(\frac{e_n}{R_F}\right) + \frac{4kT}{R_F} + \frac{(e_n 2\pi f_{-3dB} C_{IN})^2}{3}} \qquad \text{Equation 4}$$

The equations presented do not account for the finite resistance of the photodetector and in-fact assume them to be zero. So while the detector designer thus must include the goal of reducing the capacitance of the photodetector to maintain a current pulse rise time into the electrical amplifier as per the TIA design equations presented, this must been done in concert with minimizing the resistance of the detector to ensure that the resistance is small compared to the input impedance of the amplifier. This is because the detector input resistance combines with the effective input impedance of the TIA and works with the TIA input capacitance to form a time constant that further limits the bandwidth of the system below the value indicated in Equation 3. This time constant determines the speed at which current pulses can leave the photodetector and flow into the amplifier.

For the optical receiver system to be able to respond to the optical signals, all the elements of the systems must be fast enough and generally, on the order of the rise time of the electrical bandwidth of the system. The slowest of the elements will otherwise restrict the speed of the overall system leading to less peak intensity at the output of the optical receiver system. Hence the detector must be designed to have speed that that does not limit the system performance.

Thus, a brief review of the bandwidth and noise dependencies on detector capacitance for a TIA is instructive in reminding the reader that the capacitance of the photodetector is important in the design of optical detection systems.

In addition to photo-generated signal, photodetectors also produce noise due to the spontaneous generation of electron hole pairs from detector. These carriers are not due to light absorption and hence contribute to noise. They come from many parts of the detector including the surface, sidewalls, and the depleted and un-depleted bulk material of the detector. In a well-designed photodetector, these noise sources are minimized with the goal of reducing them below the amplifier noise as well as the solar background noise.

Noise obscures the ability to detect weak light because it produces a level that the electrical signal must overcome to be detected. Many techniques exist for increasing the system's effective sensitivity despite the noise, such as pulse averaging,

optical amplification, and others. Despite all these approaches a low noise photodetector and amplifier is still fundamentally essential to achieve the goal of ever-improving levels of system sensitivity to low levels of light.

In the design of optical detection systems, peak performance (speed, noise, power consumption, linearity, etc.) from the amplifier can be achieved by careful control of the parameters of the photodetector. Thus, the photodetector plays a key role in the system-level performance of the optical detection system.

DETECTOR DESIGN

One way to fabricate InGaAs photodetectors is to diffuse a junction into the planar photodetector material (Figure 3). If the detector is to be used for front-side illumination, then the anode contact is made with thin metal wires that minimize the amount of shadowing due to the contacts. The diffused junction serves to create a depletion region where photo-generated carriers drift in the built-in electric field and witinh the applied bias electric field and are collected at the contacts of the device. In areas adjacent to the depletion area there is not a strong electric field and carriers must diffuse for a period of time until they either recombine or they happen upon the depletion area of the junction and are collected. Only the latter carriers, those swept into the depletion region, contribute to the photo-generated current delivered to the terminals of the device. It takes time for the carriers outside the depletion region to eventually be collected. The distance that the carriers are away from the depletion region is a factor in how long it takes for them to be collected. There is a recombination time constant also associated with carriers that are photo-generated outside the depletion region and if they are not swept up in such time then they will recombine and contribute nothing to the terminal current. As discussed in the previous section, if they arrive to the depletion region after an extended period of time, they will no longer contribute to the peak of the pulse response that the optical receiver system was producing from the detected optical pulse because their energy is delivered later than that of the peak of the signal. The time it takes for carriers to be collected is based on their transport through the field-free, un-depleted areas of the detector (typically the absorber region) is called the “transit time” in this simple description.

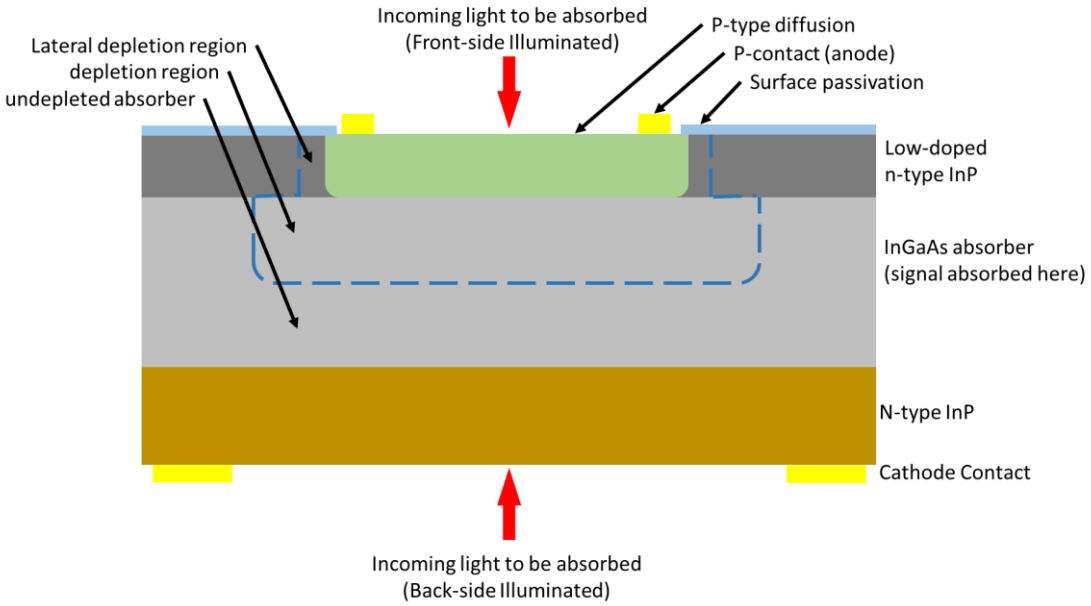

Figure 3. Planar diffusion-doped InGaAs P-I-N Photodetector shown for both Front-Side illumination (FSI) and Back-Side Illumination (BSI).

In a well-designed, planar, diffusion-doped photodetector, the capacitance is created by the properties of the diffused junction and the detector layer geometry. For the example of an InGaAs heterojunction diffused photodetector shown in Figure 3, this capacitance manifests itself in two portions, the edge capacitance of the InP cap lateral junction and the nearly parallel plate junction capacitance formed by the diffused InP cap and the material on the other side of the absorber,

be it un-depleted InGaAs absorber or the n-doped InP on the other side of the heterojunction. The material permittivity, the thickness of the depleted area, and the area of the capacitor dictates the junction capacitance of the photodetector. The total capacitance is a combination of all sources including but not limited to the edge capacitance and the junction capacitance. In large-area detectors, the junction capacitance typically dominates because the perimeter area is significantly smaller than the area of junction. To control the capacitance of the detector, a thick absorber is used so that when depleted under reverse bias, the thickness of the parallel plate capacitor formed is maximized thus reducing the dominant capacitance of the detector.

Front-side illuminated detectors have the advantage over backside illuminated detectors in that they can be used to detect optical wavelengths from 400 nm to 1700 nm while the backside illuminated detectors are limited to wavelengths longer than the absorption edge of the InP substrate. This is particularly relevant since many modulated light detection systems make use of lasers and LEDs at 850 nm, 905 nm and 940 nm where the InP substrate is very strongly absorbing thus reducing the quantum efficiency of the detector below practical limits for successful system implementation.

DETECTOR PERFORMANCE

Attollo manufactures custom and standard array products optimized for LiDAR applications. This paper will review data from one such product, Attollo's 64-channel linear array. The top-level metal layout for this array is shown in Figure 4. This array is manufactured with 64 pixels that are 7.7 mm tall and spaced on a 220 µm pitch. This array has been optimized for low cost manufacturing including special attention taken to reduce the number of mask steps needed for detector fabrication, allowances for wire bonded packaging, the use of front-side illumination, and a simplified epitaxial structure for ease of crystal growth. This paper will describe characterization of this array and discuss the role low detector capacitance plays on LiDAR system performance.

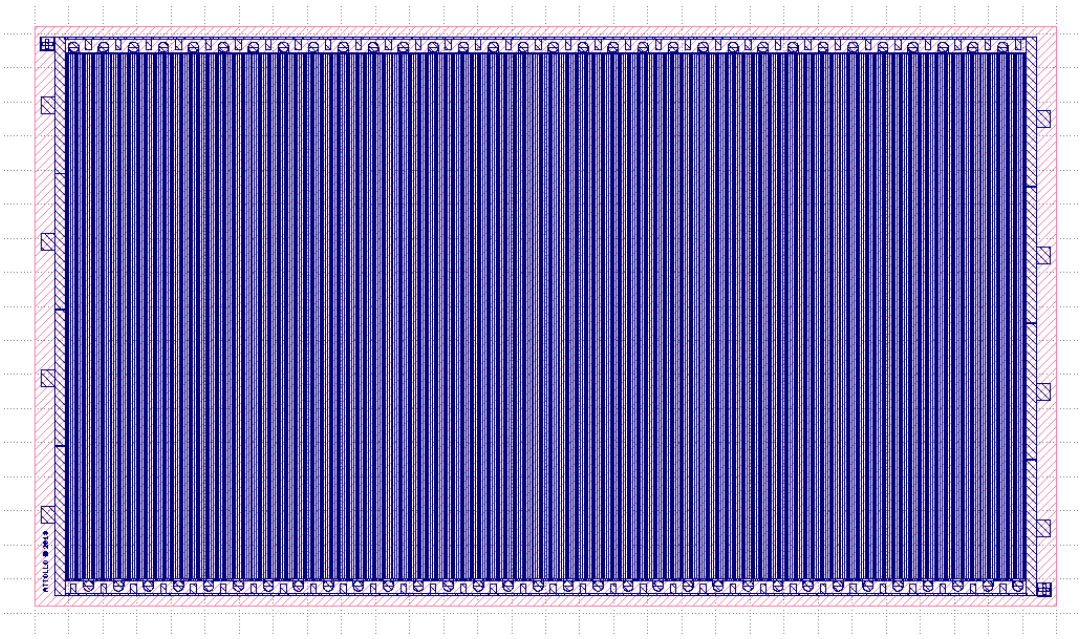

Figure 4. 64-channel 1-D LiDAR array manufactured by Attollo. Each element is 7.7 mm tall and 220 µm wide.

We measured the capacitance of devices as a function of bias voltage. Two different designs were measured; a standard low-capacitance design and an ultra low-capacitance design. The capacitance for InGaAs is often expressed as a capacitance density to enable comparison between vendors and designs and this data is shown on the left and the right of Figure *5*, respectively. At 10V reverse bias, one design achieved 37.3 pF and the other 27.2 pF. The total capacitance includes contribution from wire bond pads and other features needed for packaging. We observed that the capacitance begins to saturate at about 4V reverse bias but continues to decrease as reverse bias is increased. The normalized capacitance of the standard low-capacitance material at a nominal 10V reverse bias is 22 pF/mm^2 and 16 pF/mm^2 for the

ultra low-capacitance InGaAs at the same operating bias. Attollo has a further-optimized design for certain applications that can achieve 13 pF/mm^2 but such devices are presently not in standard production.

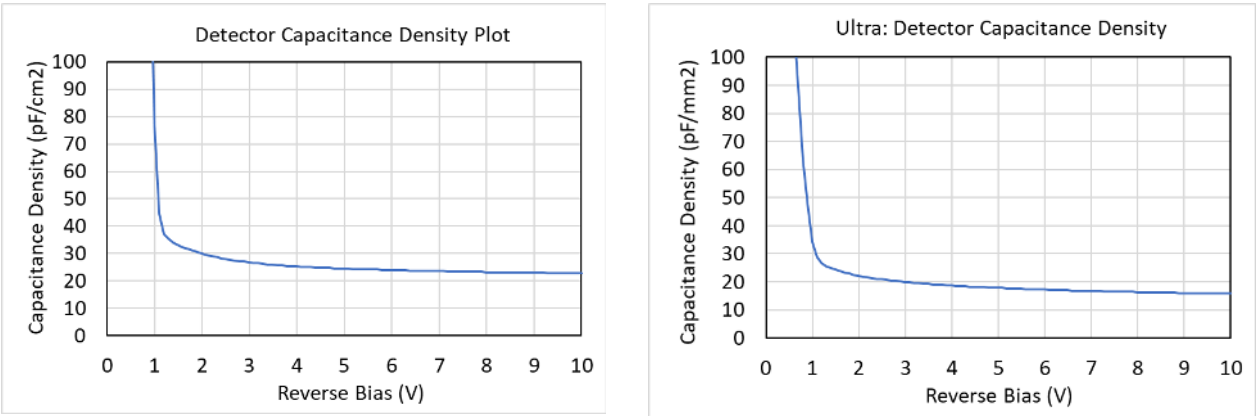

Figure 5. Detector capacitance versus voltage for Attollo's (left) standard low-capacitance and (right) ultra low-capacitance InGaAs photodetectors.

Figure 6 shows the dark current density taken for a low-capacitance InGaAs detector. At an operating voltage of 10 V reverse bias, the dark current density was measured to be just under 100 nA/cm^2, measured at 23 °C. The total dark current for the detector is close to just 2 nA. In a high-speed LiDAR system, the noise contribution from dark current will generally not be a dominant term and modeling shows that it is not a significant contributor to the total noise until it gets close to several micro-amps.

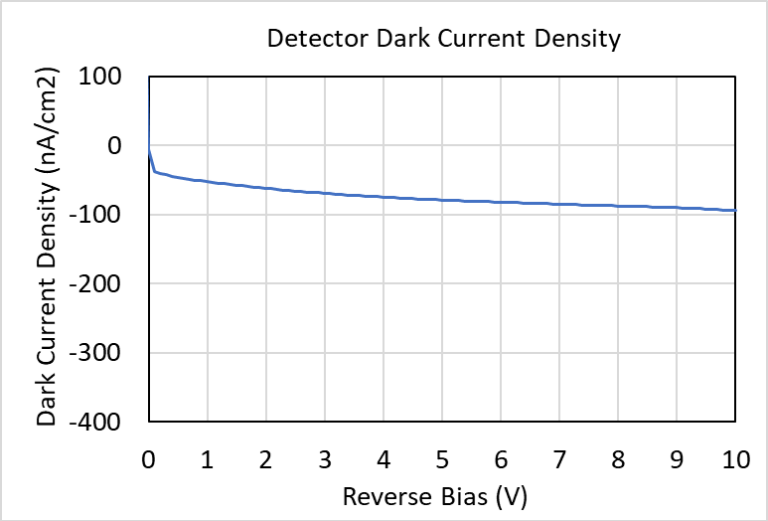

Figure 6. Dark current density measured at 23 °C for a 7.7 mm by 220 µm low-capacitance photodetector.

Analysis of the dark current measured as a function of temperature can often provide insight into the dominant dark current-generating mechanisms at play within the detector at a given operating voltage. Temperature-dependent dark current data was measured for a device from approximately +25 °C up to approximately +70 °C and is plotted in Figure 7 (left). Generating an Arrhenius plot with the same data we extracted an activation energy of 710 meV which closely matches that of the bandgap of InGaAs matched to InP. This indicates that the primary dark current component of the photodiode arises from diffusion current and that the detector material is largely free of defects that can contribute to dark current.

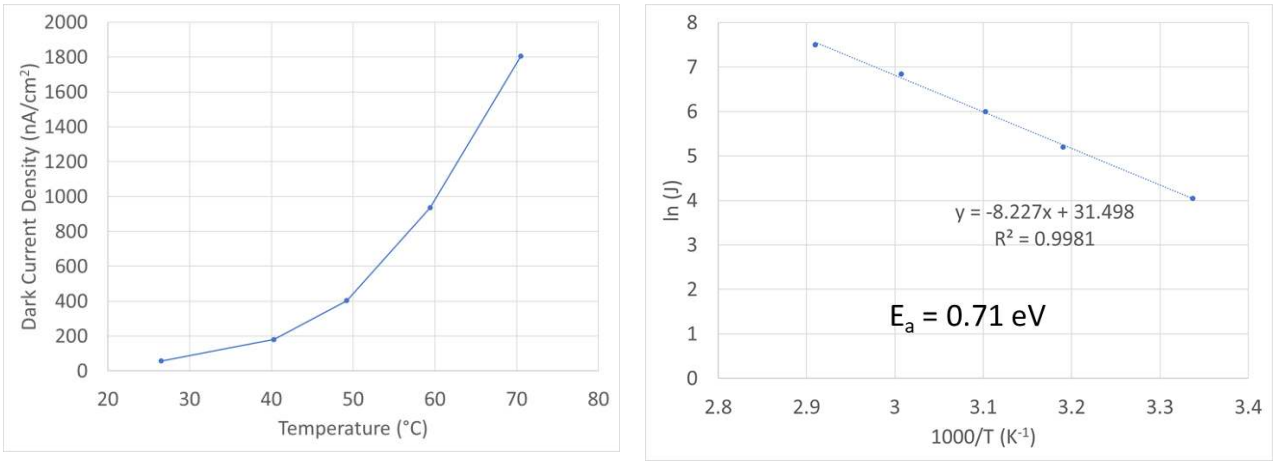

Figure 7. Temperature dependent dark current data (left) and the associated Arrhenius plot (right). The extracted activation energy was 710 meV.

A detector attribute that lends well to high volume mass production is the stability of performance after typical solder reflow profiles. This allows the detector to be a packaged on the PCB with a variety of processes without concern for degradation of the detector. One common indication that degradation has occurred is an increase in the dark current of the device. We tested our detector process and design compatibility with solder reflow by measuring the dark current of 30 test structures before and after subjecting the wafer to a solder reflow profile that included 60 seconds at 260°C. The results are shown in Figure 8. The figure shows that the dark current remains substantially unchanged before and after the reflow and is a good indication that Attollo's parts will be compatible with a variety of packaging approaches.

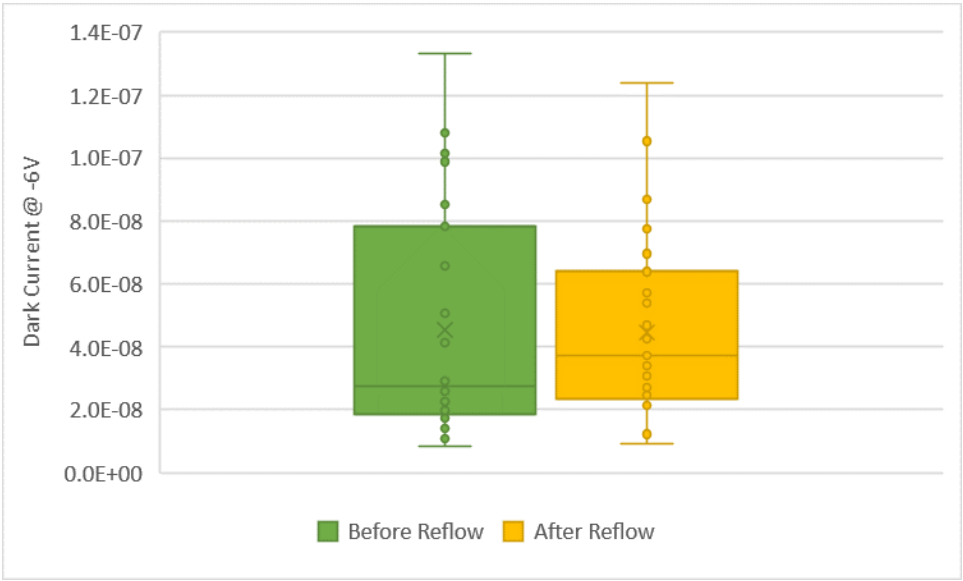

Figure 8. Stable dark current measurements of 30 test structures before and after a 60 second 260°C solder reflow profile.

In the BACKGROUND Section we reviewed the impact of detector capacitance on the bandwidth and noise of a transimpedance amplifier-based signal conditioning circuit following the detector in a LiDAR system topology as show in Figure 2. Here we will examine specific examples for two different types of systems with the data in Table 2. The first column of analysis is for the case of a single pixel for the 64-channel detector product reviewed in this paper. The pixel is 220 um by 7.7 mm and has a total capacitance of 41.5 pF at 6-volts reverse bias. In the analysis we assume that the input capacitance to the TIA is just that of the detector, a fair assumption in the case of good layout and design and when the detector capacitance is as high as those used in these examples. The second column is an example analysis for the case

of a more modestly sized square detector element measuring just 400 um on a side as may be typical in a narrow field of view rangefinding system.

In the analysis, the feedback resistance has been tuned to maximize the gain while staying within the example 3-dB limited bandwidths of 10 MHz for the LiDAR array and 30 MHz for the rangefinder. These gains are 3400 and 4000 respectively and are acceptable levels for the first stage gain in a real-world system. As a reminder, this analysis assumes that the detector has no series resistance and that the TIA feedback capacitance is set to the value that follows Equation 2 as indicated in the corresponding row of the table.

The noise analysis portion of the table shows that of the four noise terms in Equation 4, it is the input capacitance term that dominates the input referred noise of the TIA system. Even in the small FOV example it is shown that the majority of the noise comes from the detector capacitance term.

This analysis is illustrative of the importance of reducing the detector capacitance to be as low as possible to reduce noise, and that this guideline is valid across the entire range of TIA design, at least if the capacitance remains the bandwidth limit of the gain selected for the circuit.

Table 2. Example analysis on the impact of capacitance on the bandwith and noise of a TIA-based LiDAR receiver.

Detector and Package		Pixel analysis	Small FOV example
Detector Width	mm	0.22	0.4
Detector height	mm	7.70	0.4
Computed Detector Area	mm2	1.69	0.16
Detector Capacitance per unit Area	pF/mm2	24.5	24.5
Computed Detector Capacitance	pF	**41.5**	**3.92**
CDIFF - diff mode across inputs	pF	0.00	0
CD - photodiode		41.5	3.92
Ccm - common mode input to ground	pF	0.00	0
Cin - sum of sources	pF	41.50	3.92

Amplifer Performance			
Amplifier		OP-AMP	OP-AMP
GBWP	MHz	90	90
Rf: Feedback Resistance	Ohms	3400	100000
Cf	Farads	4.6E-12	2.6E-13
	pF	4.65	0.26
f3dB	Hz	1.0E+07	6.0E+06
	MHz	**10.1**	**6.0**

Noise			
i_n: ampliifer current noise	A/rt(Hz)	5.50E-15	3.50E-15
e_n amplifier voltage noise	A/rt(Hz)	4.30E-09	1.10E-09
Noise Term 1: current noise term	A/rt(Hz)	5.50E-15	3.50E-15
Noise Term 2: voltage noise term	A/rt(Hz)	1.26E-12	1.10E-14
Noise Term 3: thermal noise term	A/rt(Hz)	4.87E-24	1.66E-25
Noise Term 4: input capacitance term	A/rt(Hz)	6.52E-12	9.46E-14
Total noise	A/rt(Hz)	6.64E-12	9.53E-14

Nosie Fractions		(Term/Total)^2	(Term/Total)^2
Term 1		0.0%	0.1%
Term 2		3.6%	1.3%
Term 3		0.0%	0.0%
Term 4: Input Capacitance		96.4%	98.5%

The speed and performance of the LiDAR receiver is not only dependent on detector capacitance as other design parameters also matter for a LiDAR detector array. In the prior analysis it was stated that the series resistance of the detector was assumed to be zero ohms. Series resistance acts like additional resistance that adds to the effective input impedance of the TIA and together with the detector capacitance increases the RC time constant to slow the response the amplifier. In the

analysis of Table 2, we can compute the effective input impedance of the TIA to be about 380 ohms by using the detector capacitance and the 3-dB bandwidth. As long as the detector series resistance is substantially lower than this value, we can rely on the presented analysis.

We measured the detector series resistance by the technique used in Reference [iii]. The procedure includes plotting the forward biased I-V on a log plot and drawing a tangent line to the linear part of the log(I) vs. V curve. Next we draw a horizontal, fixed-current line at point where current change is no longer exponential. Then we mark the voltage location where the horizontal line intersects the log(I) vs. V line from the first step. Finally, we calculate the series resistance as the voltage difference divided by the fixed current. The data and procedure is shown in Figure 9. From this procedure we determine that the detector array pixels have a resistance of 2.45 Ohms. This is a good value for our application and allows us to use the prior noise and bandwidth analysis with good confidence.

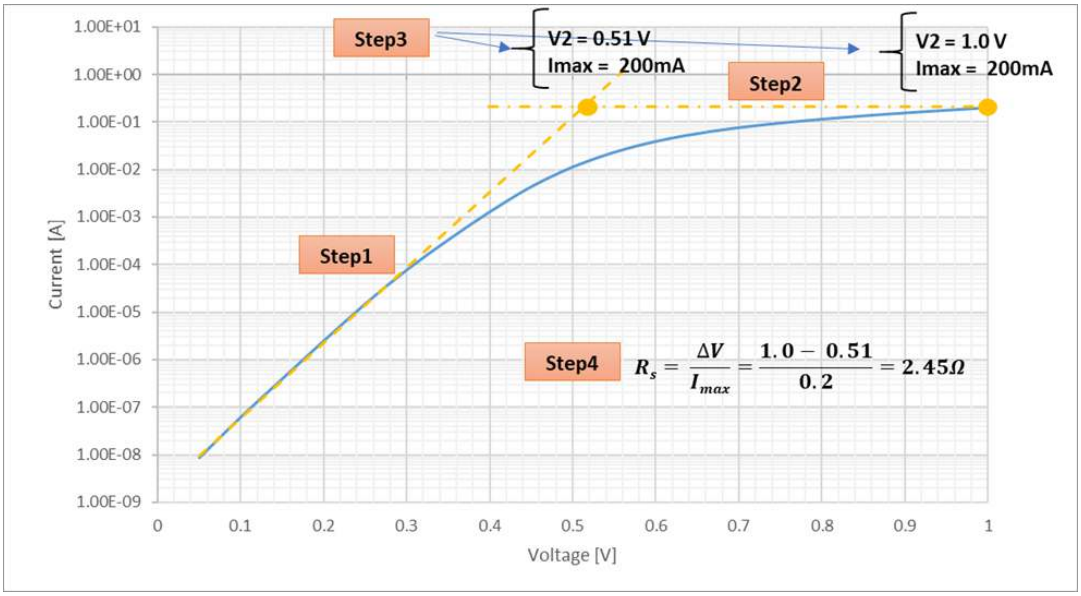

Figure 9. Forward biased method for determining the series resistance of the Attollo LiDAR detector pixel.

As was discussed in the BACKGROUND Section of this paper, in addition to detector capacitance and series resistance, the next dominant source of speed limitations originates from the design of the array itself. This is due to carrier transit time of photogenerated carriers from undepleted regions between neighboring pixels. This transit time causes carriers to be collected a point in time later than the rest of the pulse thus taking energy out of the peak of the pulse, essentially like a position dependent frequency response.

To make position dependent frequency performance measurements on our detector array, we build the test fixture shown in Figure 10. Here we have a fiber coupled laser that can be operated continuous wave (DC), pulsed, or modulated. The laser is focused using a fiber focuser onto a detector array packaged into a Leadless Chip Carrier (LCC). The detector is biased with a Bias-T to 6 volts and the RF signal is connected to a frequency spectrum analyzer. The fiber focuser can be moved from position to position on the array enabling the RF power collection at the position to be measured by the spectrum analyzer and the DC current to be measured on the source meter biasing the individual detectors. The fiber focuser creates a light spot on the detector of about 8 µm in diameter. The micro-positioner on the stage has about a 1 µm resolution.

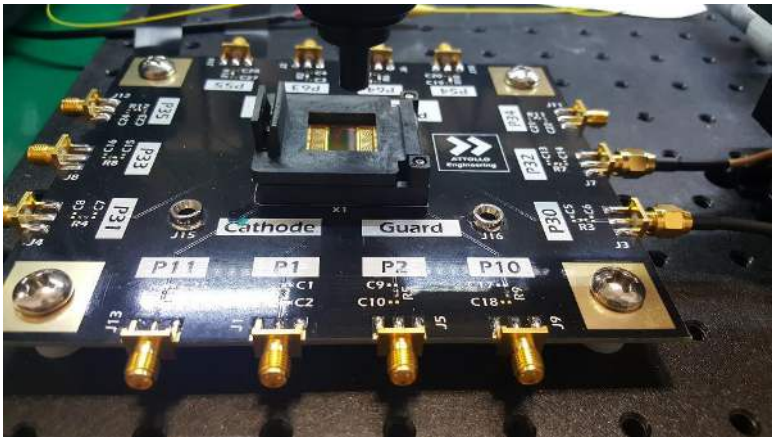

Figure 10. A picture of the Attollo RF performance characterization station showing the fiber focused laser light on the packaged 64-channel detector in an LCC.

First, we looked at the impact of the total current collection when moving the continuously driven laser from one pixel to the other. We would expect a gradual shift in current generation from one pixel to the neighbor as the spot is moved from the edge of one pixel to the next. This is exactly what we measured and is shown in Figure 11. We see that as the spot moves across the 17 µm gap from one pixel to the next, the DC current measured from each pixel changes, but the total current sum for the two elements combined is largely unchanged. This is because the carrier lifetimes in this material are long and thus the diffusion length is long compared to the 17 µm gap. The roll-off on the edges of the plot are due to shadowing from the wire anode contacts near the edge of each detector element.

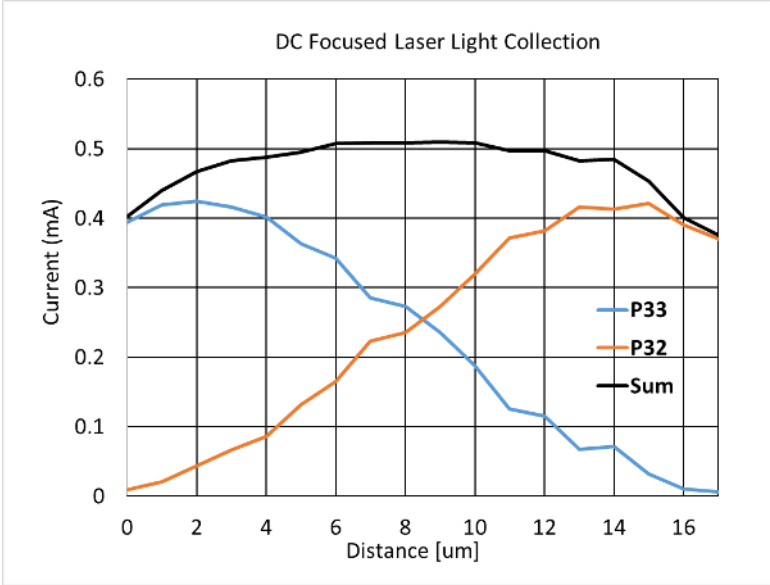

Figure 11. Plot of the continuously operated laser light collection of two neighboring pixels as the 8 um focused light spot translates from the edge of one biased detector to the next biased detector.

Though interesting, the DC measurement is not very illustrative of the LiDAR system performance because the LiDAR system is not operated as a DC system. Hence, we needed to perform a similar characterization with RF signals. To do this we modulated the laser with an RF function generator and replaced the source meter current measurement with RF power measurement via a spectrum analyzer. We blurred the laser spot to 70 µm in diameter to validate the test station. We connected an empty LCC into the test station and made a C-V measurement of the test station to get a correction term for subsequent data collection. We then placed our LiDAR array in to the setup and swept the laser modulation frequency and measured the relative response of the system with the spectrum analyzer. The results are plotted in Figure 12. We see

that the data, once corrected for the test station capacitance, is an excellent fit with the expected (dashed line) fit for a 42 pF capacitance detector. This lends confidence that our analysis and test station setup is sound.

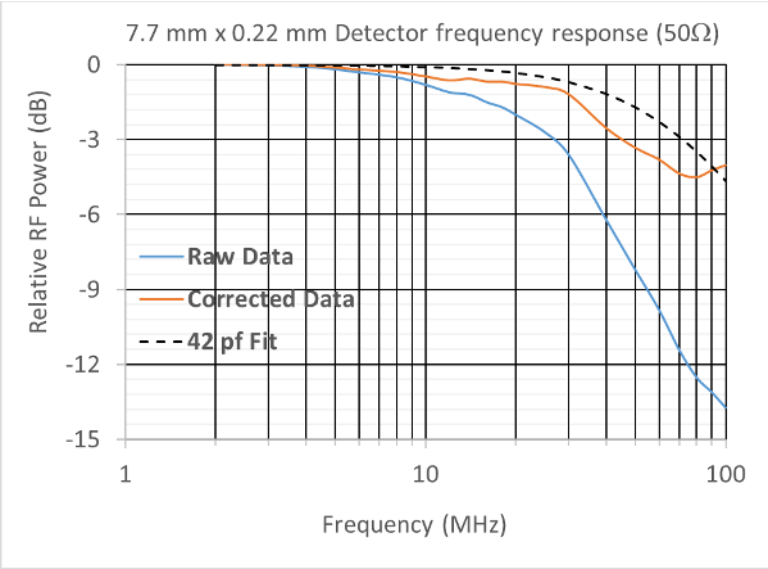

Figure 12. Swept frequency analysis of our packaged LiDAR array. The data is a good fit with the C-V capacitance measurement.

Next, we measured the RF power that is collected as the focused laser spot moves from the edge of one pixel across the 17 µm gap toward the neighboring pixel. The results are shown in Figure 13. We see that the result is very different than the CW/DC case. At 10 MHz, the power near the center drops 5dB more than the DC case and at 100 MHz, there is no measurable RF power collected. What this means is that the speed of the carrier collection in the gap is robbing RF power away from the signal and greatly attenuating the response. With the gap chosen, high frequency signals will not be collected from the very middle of the gap. This array was optimized for 10 MHz and for a laser spot much larger than 8 µm in diameter so the result is within expectations. This measurement is an instructive example of the importance of the array design for the LiDAR system performance.

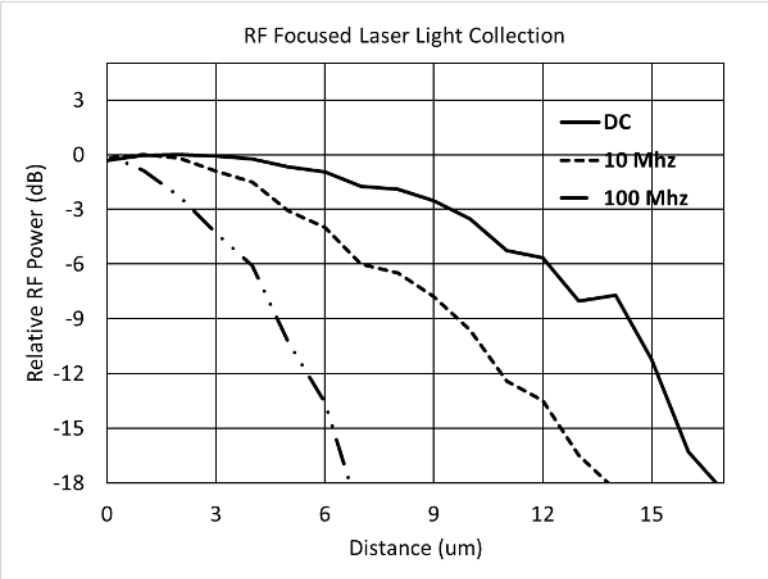

Figure 13. RF power of the signal collected by a pixel as the focused laser translates from the edge of the array pixel toward the neighboring pixel.

Next, to better develop design rules for future array production, we fabricated an array with variable pitch between detector elements and we measured the fraction of the total RF power collected from the exact center of the gap between two neighboring elements by shorting the neighbors together. This test is to demonstrate the design rules for selecting the gap size based on the RF performance required by the customers application. The results of the experiment are plotted in Figure 14. We see from the plot that as the frequency increases the necessary gap size must be reduced to collect the signal without appreciable attenuation. At 10 MHz, for example, a 17 µm gap only attenuates the signal from the center of the gap by 10% with 90% reaching the terminals of the detector. However, the same 17 µm gap loses 50% of the power at about 45 MHz. For systems operating near 100 MHz, the gaps should be maintained closer to 12.5 µm. Recall however that the laser spot is actually 8 µm so measurements for the narrower gaps will have more error because a more significant portion of the optical power is not really hitting the center of the gap, but instead is hitting closer to the detector depletion region and improving the apparent efficiency of the power collection. Never-the-less, most high volume LiDAR systems have wide FOV optics and also do not achieve tightly focused spot sizes and this mitigates the impact of the power loss in the gap between detector elements in the array.

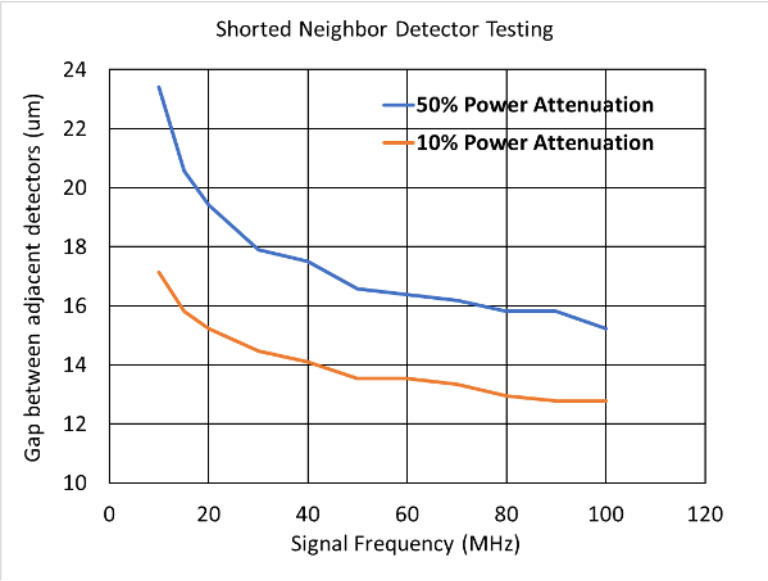

Figure 14. Plot or the total RF power collected from the center of the gap by the LIDAR array as a function of the gap spacing.

CONCLUSION

Attollo Engineering has developed low and ultra-low capacitance InGaAs with normalized capacitances of 22 pF/mm^2 and 16 pF/mm^2, respectively representing capacitance densities about ~2x to 3x lower than state-of-the-art InGaAs arrays. We have shown dark current analysis indicating high-quality material and diffusion-limited performance that achieves < 100 nA/cm^2 at 23 °C. Attollo has demonstrated that the detectors presented are solder-reflow compatible for high-volume manufacturing; showing no dark current degradation with 260 °C solder reflow profiles. RF, focused laser spot device characterization was used to validate application-specific performance of particular designs with respect to the RF power lost due to transit time in the gaps between neighboring detector elements in the array. We have shown that device designs can be tuned for the desired BW and the focused spot size of the customer's application. The InGaAs detectors presented are well suited for low-noise, high bandwidth LiDAR systems and wide field of view laser spot detection systems such as semi-active laser seekers as well as low-noise rangefinder receivers.

REFERENCES

[i] Hoelter, T.R. and J.B. Barton, Extended short-wavelength spectral response from InGaAs focal plane arrays. Proceedings of SPIE, 2003. 5074: p. 481-490.

[ii] H. Hashemi, Transimpedance Amplifiers (TIA): Choosing the Best Amplifier for the Job, Texas Instruments Application Report, SNOA942A, May 2017.

[iii] N. Rahimi, A. Patadia, D. Babic, D. Grubisic, J. Kunsch, Characterization of the Linearity of InGaAs Photodetectors Using Series Resistance, GMA/ITG-Fachtagung Sensoren und Messsysteme (2016) pp. 519-523. https://www.ama-science.org/proceedings/details/2400